This is a preprint of an article accepted for publication in ASCE Journal of Engineering Mechanics on 22 February 2012. The published article is available online at http://ascelibrary.org/doi/abs/10.1061/(ASCE)EM.1943-7889.0000423
To be cited as: Bouaanani N., Goulmot D., Miquel B. 2012. Seismic response of asymmetric rectangular liquid containing structures. ASCE Journal of Engineering Mechanics, 138(10): 1288–1297.

Seismic response of asymmetric rectangular liquid-containing structures

Najib Bouaanani, M.ASCE [1] ; Damien Goulmot [2] and Benjamin Miquel [3]

ABSTRACT

A new formulation to investigate the seismic response of symmetric and asymmetric rectangular liquid-containing structures is developed and validated in this paper. The proposed method is based on a sub-structuring approach, where the flexible liquid-containing structure is modeled using finite elements, while the impulsive effects of the fluid domain are modeled analytically through interaction forces at the fluid-structure interfaces. The technique takes account of geometrical or material asymmetry of the liquid-containing structure, fluid compressibility, and energy dissipation through reservoir bottom absorption. The formulation is presented in such a way that it can be easily coded into a practical and computationally efficient program and is applied to illustrative examples highlighting the effects of geometrical and material asymmetry on the dynamic responses of liquid-containing structures. The obtained frequency- and time-domain results are successfully validated against advanced finite element analyses.

Key words: Seismic response; Fluid-structure interaction; Liquid-containing structures; Tanks; Reservoirs; Analytical formulations; Frequency response; Time-history response; Hydrodynamic pressure; Finite elements.

[1] Associate Professor, Department of Civil, Geological and Mining Engineering, École Polytechnique de Montréal, Montréal, QC H3C 3A7, Canada
Corresponding author. E-mail: najib.bouaanani@polymtl.ca
[2] Graduate Research Assistant, Department of Civil, Geological and Mining Engineering, École Polytechnique de Montréal, Montréal, QC H3C 3A7, Canada.
[3] Graduate Research Assistant, Department of Civil, Geological and Mining Engineering, École Polytechnique de Montréal, Montréal, QC H3C 3A7, Canada.

1 Introduction

The dynamic response of liquid-containing structures has been extensively investigated since the early works of Hoskins and Jacobsen (1934), Jacobsen (1949), Werner (1949), Jacobsen and Ayre (1951), Graham and Rodriguez (1952), and Housner (1957, 1963). The continuous impetus for more refined research on this topic has been sustained by severe damage to liquid-containing structures caused by events such as the 1960 Chilean earthquakes (Steinbrugge 1963), the 1964 Alaska earthquake (Hanson 1973), the 1994 Northridge earthquake (Hall 1995), and the 1999 Turkey earthquake (Steinberg and Cruz 2004). During such events, liquid-containing structures must be damage-proof to avoid spillage of hazardous materials such as toxic chemicals and highly inflammable products. Water storage tanks are also crucial post-earthquake lifeline structures, providing water to extinguish fires occurring in the aftermath of earthquakes, as well as safe supplies of drinking water.

The authors of the earlier studies (Jacobsen 1949, Werner and Sundquist 1949, Jacobsen and Ayre 1951, Housner 1957, Housner 1963) developed analytical methods to evaluate the effects of dynamic fluid pressure assuming that the containers are rigid, and that the fluid is incompressible and inviscid, with its motion limited to small displacements. The work of Chopra (1967, 1968, 1970) on gravity dams showed that structural flexibility influences significantly the dam's interaction with the impounded reservoir, and consequently the overall seismic response. Subsequent studies on liquid-containing structures also confirmed that the flexibility of container walls affects considerably the coupled dynamic response of the fluid-container system and should thus be included in such analyses (Veletsos 1974, Veletsos and Yang 1976, Veletsos and Yang 1977, Haroun 1980, Haroun 1983, Haroun and Housner 1981a, Haroun and Housner 1981b, Balendra et al. 1982). The dynamic fluid pressures within liquid-containing structures are generally decomposed into: (i) a convective component generated by the sloshing of a portion of the fluid near the free surface, and (ii) an impulsive component generated by a portion of the fluid accelerating with the container. It has been shown that the coupling between liquid sloshing modes and container vibration modes is weak (Veletsos 1974, Haroun 1980, Haroun and Housner 1982). Consequently, convective and impulsive pressures can first be determined separately and their effects combined later to obtain the total dynamic response (Kana 1979, Malhotra et al. 2000). In practice, convective pressures are determined assuming that the container is rigid, and impulsive pressures are obtained by analyzing the interacting liquid-structure system while neglecting sloshing effects (Veletsos 1974, Haroun and Housner 1981b).

Although significant work has been dedicated to the dynamics of liquid-containing structures, there is no available practical analytical technique to evaluate the dynamic and seismic responses of asymmetric rectangular liquid-containing structures. The non-symmetry of a liquid-containing structure is common and may originate from various sources, such as

different geometries of the lateral walls, i.e. *geometric asymmetry*, as illustrated in Fig. 1, or their different constitutive materials, i.e. *material asymmetry*, due to intentional design, asymmetric damage or asymmetric retrofitting for example. In such cases, the flexibilities of the two lateral walls and consequently the associated fluid boundary conditions are no longer symmetric as assumed in available analytical approaches.

In this paper, we propose an original analytical method to investigate the dynamic and seismic responses of symmetric and asymmetric rectangular liquid-containing structures. In addition to accounting for walls' flexibility, the developed frequency- and time-domain solutions will also include the effects of water compressibility as well as energy dissipation through wave absorption at the container's bottom, two parameters which did not receive much attention in the literature relating to liquid-containing structures.

2 Governing equations

2.1 Reservoir dynamics and boundary conditions

We consider an asymmetric liquid-containing structure as illustrated in Fig. 1. For clarity, the terms structure and reservoir are used in this paper to refer to the solid and fluid domains of the system, respectively. We assume that: (i) the longitudinal dimension of the structure is sufficiently large so that it can be modeled as a two-dimensional plane-strain elasticity problem; (ii) all materials have a linear elastic behavior; (iii) the walls are flexible and have vertical faces at the interface with the reservoir; (iv) the contained liquid is compressible, inviscid, with its motion irrotational and limited to small amplitudes; (v) sediment deposits may accumulate at the reservoir bottom, (vi) gravity surface waves and convective effects are neglected. The reservoir is of length $L_\mathrm{r} = 2\,b_\mathrm{r}$ and height H_r as illustrated in Fig. 1. We adopt a Cartesian coordinate system with origin at the reservoir bottom, a horizontal axis x and a vertical axis y coincident with the axis of symmetry of the reservoir as shown in Fig. 1. We note that the structure can have a geometric and/or material asymmetry as described before.

Under the above-mentioned assumptions, the hydrodynamic pressure $p(x, y, t)$ is governed by the classical wave equation

$$\nabla^2 p = \frac{1}{C_\mathrm{r}^2}\,\frac{\partial^2 p}{\partial t^2} \tag{1}$$

where ∇^2 is the Laplace differential operator, t the time variable, and C_r the compression wave velocity. Considering a unit horizontal harmonic ground accelerations $\ddot{u}_\mathrm{g}(t) = \mathrm{e}^{\mathrm{i}\omega t}$, the hydrodynamic pressure in the reservoir can be expressed in the frequency domain as $p(x, y, t) = \bar{p}(x, y, \omega)\,\mathrm{e}^{\mathrm{i}\omega t}$, where $\bar{p}(x, y, \omega)$ is a complex-valued Frequency Response Function (FRF). Introducing this transformation into Eq. (1) yields the classical Helmholtz equa-

tion

$$\nabla^2 \bar{p} + \frac{\omega^2}{C_{\mathrm{r}}^2}\,\bar{p} = 0 \tag{2}$$

The empty structure is first modeled using finite elements. The dynamic equilibrium of the structure-reservoir system can then be expressed in the frequency domain as

$$\left[-\omega^2\,\mathbf{M} + (1 + \mathrm{i}\,\eta_{\mathrm{s}})\,\mathbf{K}\right]\overline{\mathbf{U}}(\omega) = -\mathbf{M}\,\mathbf{1} + \bar{\mathbf{F}}_{\mathrm{h}}(\omega) \tag{3}$$

where $\overline{\mathbf{U}}$ is a column-vector containing the FRFs of the structure's nodal displacements relative to the ground, $\mathbf{M}$ and $\mathbf{K}$ are the structure's mass and stiffness matrices, respectively, η_{s} is the structural hysteretic damping factor assumed constant, $\bar{\mathbf{F}}_{\mathrm{h}}$ is a column-vector containing the FRFs of hydrodynamic pressure loads exerted at lateral walls, and $\mathbf{1}$ is a column-vector with the same dimension as the vector of nodal relative displacements, containing zeros except along horizontal degrees of freedom which correspond to the direction of earthquake excitation. Using modal superposition, the FRFs of relative displacement and acceleration components at a given point of the structure with coordinates (x, y) can be expressed as

$$\bar{u}(x,y,\omega) = \sum_{j=1}^{m_{\mathrm{s}}} \psi_j^{(x)}(x,y)\,\bar{Z}_j(\omega)\,; \qquad \bar{\ddot{u}}(x,y,\omega) = -\omega^2 \sum_{j=1}^{m_{\mathrm{s}}} \psi_j^{(x)}(x,y)\,\bar{Z}_j(\omega) \tag{4}$$

$$\bar{v}(x,y,\omega) = \sum_{j=1}^{m_{\mathrm{s}}} \psi_j^{(y)}(x,y)\,\bar{Z}_j(\omega)\,; \qquad \bar{\ddot{v}}(x,y,\omega) = -\omega^2 \sum_{j=1}^{m_{\mathrm{s}}} \psi_j^{(y)}(x,y)\,\bar{Z}_j(\omega) \tag{5}$$

where $\bar{u}$ and $\bar{v}$ denote the horizontal and vertical relative displacements, respectively, $\bar{\ddot{u}}$ and $\bar{\ddot{v}}$ the horizontal and vertical accelerations, respectively, $\psi_j^{(x)}$ and $\psi_j^{(y)}$ the x– and y–components of the $j^{\,\mathrm{th}}$ mode shape of the empty structure, $\bar{Z}_j$ the generalized coordinate, and m_{s} the number of structural mode shapes included in the analysis. The hydrodynamic pressure FRF $\bar{p}$ can be decomposed as (Fenves and Chopra 1984, Bouaanani and Lu 2009)

$$\bar{p}(x,y,\omega) = \bar{p}_0(x,y,\omega) - \omega^2 \sum_{j=1}^{m_{\mathrm{s}}} \bar{Z}_j(\omega)\,\bar{p}_j(x,y,\omega) \tag{6}$$

where $\bar{p}_0$ is the FRF for hydrodynamic pressure due to rigid body motion of the empty structure, and where $\bar{p}_j$ is the FRF corresponding to hydrodynamic pressure due to horizontal accelerations $\psi_j^{(x)}(-b_{\mathrm{r}}, y)$ and $\psi_j^{(x)}(b_{\mathrm{r}}, y)$ along structural mode shape j of the empty structure. The boundary conditions to be satisfied by FRFs $\bar{p}_0$ and $\bar{p}_j$ are as follows:

– *At the structure-reservoir vertical interfaces*

These boundary conditions are based on compatibility between hydrodynamic pressures and displacements at the lateral walls located at $x = -b_{\mathrm{r}}$ and $x = b_{\mathrm{r}}$, yielding

$$\frac{\partial \bar{p}_0}{\partial x}(-b_{\mathrm{r}},y,\omega) = -\rho_{\mathrm{r}}\,; \qquad \frac{\partial \bar{p}_j}{\partial x}(-b_{\mathrm{r}},y,\omega) = -\rho_{\mathrm{r}}\,\psi_j^{(x)}(-b_{\mathrm{r}},y) \tag{7}$$

$$\frac{\partial \bar{p}_0}{\partial x}(b_{\mathrm{r}},y,\omega) = -\rho_{\mathrm{r}}\,; \qquad \frac{\partial \bar{p}_j}{\partial x}(b_{\mathrm{r}},y,\omega) = -\rho_{\mathrm{r}}\,\psi_j^{(x)}(b_{\mathrm{r}},y) \tag{8}$$

where ρ_{r} is the mass density of water.

– *At reservoir free surface*

Neglecting the effects of gravity waves at reservoir free surface, hydrodynamic pressures at this location are assumed null

$$\bar{p}_0(x, H_{\mathrm{r}}, \omega) = \bar{p}_j(x, H_{\mathrm{r}}, \omega) = 0 \tag{9}$$

– *At reservoir bottom*

An absorptive boundary condition introduced by Hall and Chopra (1982) to account for energy dissipation through one-dimensional partial absorption of incident compression waves normal to the reservoir boundary

$$\frac{\partial \bar{p}_0}{\partial y}(x, 0, \omega) = \mathrm{i}\,\omega q\,\bar{p}_0(x, 0, \omega)\,; \qquad \frac{\partial \bar{p}_j}{\partial y}(x, 0, \omega) = \mathrm{i}\,\omega q\,\bar{p}_j(x, 0, \omega) \tag{10}$$

where q is a damping coefficient defined at the reservoir bottom as

$$q = \frac{\rho_{\mathrm{r}}}{\rho_{\mathrm{f}}\, C_{\mathrm{f}}} \tag{11}$$

with ρ_{f} and C_{f} denoting the mass density and the compression wave velocity within the reservoir foundation, respectively. The portion of the wave amplitude reflected back to the reservoir is represented by the wave reflection coefficient α defined by

$$\alpha = \frac{1 - q\, C_{\mathrm{r}}}{1 + q\, C_{\mathrm{r}}} \tag{12}$$

where α generally varies from 0 for high wave absorption, to 1 for high wave reflection. In the latter case, Eq. (10) simplifies to

$$\frac{\partial \bar{p}_0}{\partial y}(x, 0, \omega) = \frac{\partial \bar{p}_j}{\partial y}(x, 0, \omega) = 0 \tag{13}$$

2.2 New formulation for coupled vibrations of structure-reservoir systems

Using Eq. (2) and the above-mentioned boundary conditions, we show in Appendix A that FRFs $\bar{p}_0$ and $\bar{p}_j$ can be expressed as

$$\bar{p}_0(x, y, \omega) = \rho_{\mathrm{r}} H_{\mathrm{r}} \sum_{n=1}^{m_{\mathrm{r}}} \frac{\lambda_n^2(\omega)\Big[I_{0\,n}^{-}(\omega)\, X_n^{-}(x, \omega) - I_{0\,n}^{+}(\omega)\, X_n^{+}(x, \omega)\Big]}{\beta_n(\omega)\, \kappa_n(\omega)\, \sinh[b_{\mathrm{r}}\kappa_n(\omega)] \cosh[b_{\mathrm{r}}\kappa_n(\omega)]}\, Y_n(y, \omega) \tag{14}$$

$$\bar{p}_j(x, y, \omega) = \rho_{\mathrm{r}} H_{\mathrm{r}} \sum_{n=1}^{m_{\mathrm{r}}} \frac{\lambda_n^2(\omega)\Big[I_{j\,n}^{-}(\omega)\, X_n^{-}(x, \omega) - I_{j\,n}^{+}(\omega)\, X_n^{+}(x, \omega)\Big]}{\beta_n(\omega)\, \kappa_n(\omega)\, \sinh[b_{\mathrm{r}}\kappa_n(\omega)] \cosh[b_{\mathrm{r}}\kappa_n(\omega)]}\, Y_n(y, \omega) \tag{15}$$

in which the parameters $\beta_n(\omega)$, $\kappa_n(\omega)$, $X_n^{-}(x, \omega)$, and $X_n^{+}(x, \omega)$ are given by Eqs. (54), (56), (67) and (68) of Appendix A, respectively, and where the integrals $I_{0\,n}^{-}(\omega)$, $I_{0\,n}^{+}(\omega)$, $I_{j\,n}^{-}(\omega)$

and $I^{+}_{j\,n}(\omega)$ are obtained from Eqs. (61) and (62) of Appendix A as

$$I^{-}_{0\,n}(\omega) = I^{+}_{0\,n}(\omega) = \frac{1}{H_{\mathrm{r}}}\int_0^{H_{\mathrm{r}}} Y_n(y,\omega)\,\mathrm{d}y$$
$$= \frac{\mathrm{i}\,\mathrm{e}^{-\mathrm{i}H_{\mathrm{r}}\lambda_n(\omega)}}{H_{\mathrm{r}}\lambda_n^2(\omega)}\Big[\lambda_n(\omega) - \omega q + \omega q \mathrm{e}^{\mathrm{i}H_{\mathrm{r}}\lambda_n(\omega)}\Big] \tag{16}$$

$$I^{-}_{j\,n}(\omega) = \frac{1}{H_{\mathrm{r}}}\int_0^{H_{\mathrm{r}}} \psi_j^{(x)}(-b_{\mathrm{r}},y)\,Y_n(y,\omega)\,\mathrm{d}y \tag{17}$$

$$I^{+}_{j\,n}(\omega) = \frac{1}{H_{\mathrm{r}}}\int_0^{H_{\mathrm{r}}} \psi_j^{(x)}(b_{\mathrm{r}},y)\,Y_n(y,\omega)\,\mathrm{d}y \tag{18}$$

We note that

$$I^{-}_{j\,n}(\omega) = 0 \quad \text{when the wall at } x=-b_{\mathrm{r}} \text{ is rigid} \tag{19}$$
$$I^{+}_{j\,n}(\omega) = 0 \quad \text{when the wall at } x=b_{\mathrm{r}} \text{ is rigid} \tag{20}$$

Evaluating the FRFs $\bar{p}_0$ and $\bar{p}_j$ at the structure's vertical walls, i.e. $x=-b_{\mathrm{r}}$ and $x=b_{\mathrm{r}}$, gives

$$\bar{p}_0(-b_{\mathrm{r}},y,\omega) = \rho_{\mathrm{r}}H_{\mathrm{r}}\sum_{n=1}^{m_{\mathrm{r}}} \frac{\lambda_n^2(\omega)\Big\{\cosh[2\,b_{\mathrm{r}}\kappa_n(\omega)]-1\Big\}\,I_{0\,n}(\omega)}{\beta_n(\omega)\,\kappa_n(\omega)\,\sinh[b_{\mathrm{r}}\kappa_n(\omega)]\,\cosh[b_{\mathrm{r}}\kappa_n(\omega)]}\,Y_n(y,\omega) \tag{21}$$

$$\bar{p}_j(-b_{\mathrm{r}},y,\omega) = \rho_{\mathrm{r}}H_{\mathrm{r}}\sum_{n=1}^{m_{\mathrm{r}}} \frac{\lambda_n^2(\omega)\Big\{I^{-}_{j\,n}(\omega)\cosh[2\,b_{\mathrm{r}}\kappa_n(\omega)]-I^{+}_{j\,n}(\omega)\Big\}}{\beta_n(\omega)\,\kappa_n(\omega)\,\sinh[b_{\mathrm{r}}\kappa_n(\omega)]\,\cosh[b_{\mathrm{r}}\kappa_n(\omega)]}\,Y_n(y,\omega) \tag{22}$$

and

$$\bar{p}_0(b_{\mathrm{r}},y,\omega) = -\bar{p}_0(-b_{\mathrm{r}},y,\omega) \tag{23}$$

$$\bar{p}_j(b_{\mathrm{r}},y,\omega) = \rho_{\mathrm{r}}H_{\mathrm{r}}\sum_{n=1}^{m_{\mathrm{r}}} \frac{\lambda_n^2(\omega)\Big\{I^{-}_{j\,n}(\omega)-I^{+}_{j\,n}(\omega)\,\cosh[2\,b_{\mathrm{r}}\kappa_n(\omega)]\Big\}}{\beta_n(\omega)\,\kappa_n(\omega)\,\sinh[b_{\mathrm{r}}\kappa_n(\omega)]\cosh[b_{\mathrm{r}}\kappa_n(\omega)]}\,Y_n(y,\omega) \tag{24}$$

If water is assumed incompressible, Eq. (56) simplifies to

$$\kappa_n = \lambda_n = \frac{(2n-1)\,\pi}{2H_{\mathrm{r}}} \tag{25}$$

and hydrodynamic pressures $\bar{p}_0$ and $\bar{p}_j$ become

$$\bar{p}_0(-b_{\mathrm{r}},y) = \frac{4\rho_{\mathrm{r}}H_{\mathrm{r}}}{\pi^2}\sum_{n=1}^{m_{\mathrm{r}}} \frac{(-1)^{n-1}\Big[\cosh(2\,b_{\mathrm{r}}\kappa_n)-1\Big]}{(2n-1)^2\,\sinh(b_{\mathrm{r}}\kappa_n)\,\cosh(b_{\mathrm{r}}\kappa_n)}\,\cos(\lambda_n\,y) \tag{26}$$

$$\bar{p}_j(-b_{\mathrm{r}},y) = \frac{2\rho_{\mathrm{r}}H_{\mathrm{r}}}{\pi}\sum_{n=1}^{m_{\mathrm{r}}} \frac{\Big[I^{-}_{j\,n}\cosh(2\,b_{\mathrm{r}}\kappa_n)-I^{+}_{j\,n}\Big]}{(2n-1)\,\sinh(b_{\mathrm{r}}\kappa_n)\,\cosh(b_{\mathrm{r}}\kappa_n)}\,\cos(\lambda_n\,y) \tag{27}$$

and

$$\bar{p}_0(b_\mathrm{r}, y) = -\bar{p}_0(-b_\mathrm{r}, y, \omega) \tag{28}$$

$$\bar{p}_j(b_\mathrm{r}, y) = \frac{2\rho_\mathrm{r} H_\mathrm{r}}{\pi} \sum_{n=1}^{m_\mathrm{r}} \frac{\left[I_{j\,n}^{-} - I_{j\,n}^{+} \cosh(2\, b_\mathrm{r}\kappa_n)\right]}{(2n-1)\, \sinh(b_\mathrm{r}\kappa_n) \cosh(b_\mathrm{r}\kappa_n)} \cos(\lambda_n\, y) \tag{29}$$

The FRF for total hydrodynamic pressure is given by Eq. (6) where the vector $\bar{\mathbf{Z}}$ of generalized coordinates $\bar{Z}_j$, $j = 1 \ldots m_\mathrm{s}$, is obtained by solving the system of equations

$$\bar{\mathbf{S}}\, \bar{\mathbf{Z}} = \bar{\mathbf{Q}} \tag{30}$$

in which elements of matrices $\bar{\mathbf{S}}$ and $\bar{\mathbf{Q}}$ are obtained for $n = 1 \ldots m_\mathrm{s}$ and $j = 1 \ldots m_\mathrm{s}$ as

$$\bar{S}_{nj}(\omega) = \Big[-\omega^2 + \left(1 + \mathrm{i}\,\eta_\mathrm{s}\right) \omega_n^2 \Big] \delta_{nj} + \omega^2 \left[\int_0^{H_\mathrm{r}} \bar{p}_j(b_\mathrm{r}, y, \omega)\, \psi_n^{(x)}(b_\mathrm{r}, y)\, \mathrm{d}y - \int_0^{H_\mathrm{r}} \bar{p}_j(-b_\mathrm{r}, y, \omega)\, \psi_n^{(x)}(-b_\mathrm{r}, y)\, \mathrm{d}y \right] \tag{31}$$

$$\bar{Q}_n(\omega) = -\, \boldsymbol{\psi}_n^\mathrm{T}\, \mathbf{M}\, \mathbf{1} + \int_0^{H_\mathrm{r}} \bar{p}_0(b_\mathrm{r}, y, \omega)\, \psi_n^{(x)}(b_\mathrm{r}, y)\, \mathrm{d}y - \int_0^{H_\mathrm{r}} \bar{p}_0(-b_\mathrm{r}, y, \omega)\, \psi_n^{(x)}(-b_\mathrm{r}, y)\, \mathrm{d}y \tag{32}$$

where δ denotes the Kronecker symbol and ω_n is the vibration frequency corresponding to structural mode shape $\boldsymbol{\psi}_n$ of the structure without water. A convergence study must be conducted to determine the sufficient numbers m_s and m_r of structural and reservoir mode shapes to be included into each specific analysis. We note that if the containing structure is symmetric, Eqs. (31) and (32) simplify to

$$\bar{S}_{nj}(\omega) = \Big[-\omega^2 + \left(1 + \mathrm{i}\,\eta_\mathrm{s}\right) \omega_n^2 \Big] \delta_{nj} + 2\,\omega^2 \int_0^{H_\mathrm{r}} \bar{p}_j(b_\mathrm{r}, y, \omega)\, \psi_n^{(x)}(b_\mathrm{r}, y)\, \mathrm{d}y \tag{33}$$

$$\bar{Q}_n(\omega) = -\, \boldsymbol{\psi}_n^\mathrm{T}\, \mathbf{M}\, \mathbf{1} + 2 \int_0^{H_\mathrm{r}} \bar{p}_0(b_\mathrm{r}, y, \omega)\, \psi_n^{(x)}(b_\mathrm{r}, y)\, \mathrm{d}y \tag{34}$$

The structural displacement and acceleration time-history responses to a ground acceleration $\ddot{u}_\mathrm{g}(t)$ can be obtained as

$$u(x, y, t) = \sum_{j=1}^{m_\mathrm{s}} \psi_j^{(x)}(x, y)\, Z_j(t)\,; \qquad \ddot{u}(x, y, t) = \sum_{j=1}^{m_\mathrm{s}} \psi_j^{(x)}(x, y)\, \ddot{Z}_j(t) \tag{35}$$

$$v(x, y, t) = \sum_{j=1}^{m_\mathrm{s}} \psi_j^{(y)}(x, y)\, Z_j(t)\,; \qquad \ddot{v}(x, y, t) = \sum_{j=1}^{m_\mathrm{s}} \psi_j^{(y)}(x, y)\, \ddot{Z}_j(t) \tag{36}$$

where the time-domain generalized coordinates Z_j are given by the Fourier integrals

$$Z_j(t) = \frac{1}{2\pi}\int_{-\infty}^{\infty} \bar{Z}_j(\omega)\,\bar{\ddot{u}}_{\mathrm{g}}(\omega)\,\mathrm{e}^{\mathrm{i}\omega t}\,\mathrm{d}\omega\,; \qquad \ddot{Z}_j(t) = -\frac{1}{2\pi}\int_{-\infty}^{\infty} \omega^2\bar{Z}_j(\omega)\,\bar{\ddot{u}}_{\mathrm{g}}(\omega)\,\mathrm{e}^{\mathrm{i}\omega t}\,\mathrm{d}\omega \quad (37)$$

in which $\bar{\ddot{u}}_{\mathrm{g}}(\omega)$ is the Fourier transform of the ground acceleration $\ddot{u}_{\mathrm{g}}(t)$

$$\bar{\ddot{u}}_{\mathrm{g}}(\omega) = \int_0^{t_a} \ddot{u}_{\mathrm{g}}(t)\,\mathrm{e}^{-\mathrm{i}\omega t}\,\mathrm{d}t \quad (38)$$

with t_a denoting the time duration of the applied accelerogram.

Based on these relations, other quantities of interest can also be determined. For example, the shear forces at a given horizontal cutting section at position y_{A} of each wall can also be obtained by expressing the dynamic equilibrium of the wall's portion above the cutting section, yielding

$$V^-(y_{\mathrm{A}},t) = \int_{y_{\mathrm{A}}}^{H_{\mathrm{r}}} p(-b_{\mathrm{r}},y,t)\,\mathrm{d}y - \iint_{\mathcal{A}^-(y_{\mathrm{A}})} \rho_{\mathrm{s}}(x,y)\Big[\ddot{u}_{\mathrm{g}}(t)+\ddot{u}(x,y,t)\Big]\,\mathrm{d}x\,\mathrm{d}y \quad (39)$$

$$V^+(y_{\mathrm{A}},t) = \int_{y_{\mathrm{A}}}^{H_{\mathrm{r}}} p(b_{\mathrm{r}},y,t)\,\mathrm{d}y - \iint_{\mathcal{A}^+(y_{\mathrm{A}})} \rho_{\mathrm{s}}(x,y)\Big[\ddot{u}_{\mathrm{g}}(t)+\ddot{u}(x,y,t)\Big]\,\mathrm{d}x\,\mathrm{d}y \quad (40)$$

where V^- and V^+ is the shear forces at the left and right walls of the liquid container, respectively, $\mathcal{A}^-$ and $\mathcal{A}^+$ are the areas of the portions located above the cutting sections of the left and right walls, respectively, and ρ_{s} is the density of the constitutive material(s) of the liquid container.

3 Validation examples

The dynamic response of symmetric and asymmetric liquid-containing structures are investigated in this section to validate the proposed method and illustrate its application. The description as well as the frequency- and time-domain analyses of the studied systems are presented in the next two subsections.

3.1 Geometrically asymmetric wall-water system

In this section, we investigate the geometrically asymmetric wall-water system illustrated in Fig. 2. The following properties are adopted for the structure's material: modulus of elasticity $E_{\mathrm{s}} = 25\,\mathrm{GPa}$, Poisson's ratio $\nu_{\mathrm{s}} = 0.2$, and mass density $\rho_{\mathrm{s}} = 2400\,\mathrm{kg/m^3}$. The reservoir contains water of mass density $\rho_{\mathrm{r}} = 1000\,\mathrm{kg/m^3}$, and has a height $H_{\mathrm{r}} = 20\,\mathrm{m}$ and a length $L_{\mathrm{r}} = 20\,\mathrm{m}$. Water is considered compressible with a velocity of pressure waves $C_{\mathrm{r}} = 1440\,\mathrm{m/s}$. A constant structural hysteretic damping factor $\eta_{\mathrm{s}} = 0.1$ is assumed. To obtain

the mode shapes ψ_j, $j = 1 \ldots m_s$, of the walls without water and corresponding modal participation factors, the structures are discretized into 8-node plane-strain solid finite elements using the software ADINA (2010). Fig. 3 (a) illustrates the finite element mesh used. Application of the proposed method described in Section 2.2 reveals that frequency response convergence up to 20 Hz requires that the first eight modes of the empty structure be included in the analysis, i.e. $m_s = 8$. Fig. 4 illustrates the first eight mode shapes given by ADINA (2010) as well as the corresponding frequencies and horizontal effective modal masses expressed in percentage of total mass of the walls. As can be seen, mode 6 is a vertical mode, and can therefore be neglected in the analysis. We also note that a wide frequency range up to 20 Hz was studied for purpose of illustration although a lower cutting frequency could have been selected considering the usual frequency content of interest under seismic excitation. The same frequency range will be used in the next examples. To validate the results, we conduct a finite element analysis where both the walls and the reservoir are modeled using 8-node plane strain and 8-node potential-based finite elements programmed in ADINA (2010), respectively. Fig. 3 (b) illustrates the finite element model used. In this case, dynamic interaction between the walls and the reservoir is achieved through fluid-structure interface elements and a potential-based formulation of the fluid domain (Everstine 1981, Bouaanani and Lu 2009).

Figure 5 shows the obtained FRFs of nondimensionalized scaled hydrodynamic pressures $|\bar{p}/(\rho_r g H_r)|$ and scaled horizontal relative displacements $|\bar{u}/u_{st}|$ where u_{st} is the lateral static displacement under the effect of hydrostatic pressure. The results are determined at points A, B, and C located on the left wall, and points A', B' and C' belonging to the right wall as indicated in Fig. 3. The vertical positions of the points are $y_A = y_{A'} = 1$ m, $y_B = y_{B'} = 10$ m, $y_C = 24$ m and $y_{C'} = 28$ m. The FRFs in Fig. 5 clearly show that the results of the proposed method are in excellent agreement with the finite element solutions over a wide frequency range up to 20 Hz. The proposed method is then used to determine the FRFs including a reflection wave coefficient $\alpha = 0.2$ at reservoir's bottom. The obtained FRFs are superposed to those in Fig. 5 and show that, in this case, the influence of reservoir bottom absorption affects mainly hydrodynamic pressures at higher frequencies larger than 10 Hz. The techniques described previously are also applied next to determine hydrodynamic pressure profiles corresponding to frequencies $0.8\ \tilde{f}_1$ and $1.2\ \tilde{f}_1$, where $\tilde{f}_1$ denotes the coupled vibration frequency of the wall-water system. The obtained profiles presented in Fig. 6 confirm that the proposed procedure yields excellent results when compared to advanced finite element formulations.

Next, we investigate the performance of the proposed method in assessing the seismic response of the previously described wall-water system. Fig. 7 illustrates the horizontal acceleration component of Imperial Valley earthquake (1940) at El Centro selected to conduct the analyses using the proposed and finite element techniques described above. The obtained time-histories of nondimensionalized horizontal relative displacements $|u/u_{st}|$ at points C and C' are shown in Fig. 8 (a) and (b). Fig. 8 (c) and (d) illustrate the nondimensionalized shear

forces V/F_{stat} at sections A and A' where $F_{\text{stat}} = \rho_{\text{r}} g H_{\text{r}}^2/2$ denotes the hydrostatic force. Fig. 8 clearly shows that the time-history responses predicted by the proposed method are almost identical to those from finite element analyses.

3.2 Materially asymmetric tank-reservoir system

We consider the tank-reservoir system illustrated in Fig. 9. The tank has a material asymmetry due to the retrofitting of one of its damaged lateral walls using a high performance material. The following properties are adopted for the structure's materials: moduli of elasticity of the original and reinforcing materials $E_{\text{s}}^{(1)} = 25\,\text{GPa}$ and $E_{\text{s}}^{(2)} = 55\,\text{GPa}$, respectively, Poisson's ratio $\nu_{\text{s}} = 0.2$, and mass density $\rho_{\text{s}} = 2400\,\text{kg/m}^3$. The tank is filled with water with a mass density $\rho_{\text{r}} = 1000\,\text{kg/m}^3$ up to a height $H_{\text{r}} = 10\,\text{m}$. The length of the reservoir is $L_{\text{r}} = 18\,\text{m}$. Water is considered compressible with a velocity of pressure waves $C_{\text{r}} = 1440\,\text{m/s}$. A constant structural hysteretic damping factor $\eta_{\text{s}} = 0.1$ is assumed. Fig. 10 (a) illustrates the finite element model of the empty tank used to obtain the modal properties required for the proposed method, while Fig. 3 (b) shows the tank-reservoir system's finite element model constructed for comparison purposes. 8-node solid and fluid finite elements programmed in ADINA (2010) are used as in the previous models.

In this case, we show that the first six modes of the empty reinforced tank are to be included in the analysis for convergence up to $20\,\text{Hz}$, i.e. $m_{\text{s}} = 6$. Fig. 11 presents the six mode shapes of the empty reinforced tank obtained using ADINA (2010) as well as the corresponding frequencies and horizontal effective modal masses expressed in percentage of total mass of the empty tank. By comparing these modes to those of the original symmetric tank, we observe that asymmetry affects the frequencies of modes 2, 4 and 6, as well as the corresponding modal masses which are now non-null.

The dynamic response of the reinforced tank-reservoir system is then studied using the previously described analytical and finite element models shown in Figs. 10 (a) and (b). Fig. 12 presents the resulting FRFs of nondimensionalized hydrodynamic pressures $|\bar{p}/(\rho_{\text{r}} g H_{\text{r}})|$ obtained at points A, B, A' and B', as well as the nondimensionalized horizontal relative displacements $|\bar{u}/u_{\text{st}}|$ at points C and C'. The positions of the points are illustrated in Fig. 10 and are located at $y_{\text{A}} = y_{\text{A'}} = 0.5\,\text{m}$, $y_{\text{B}} = y_{\text{B'}} = 5\,\text{m}$, and $y_{\text{C}} = y_{\text{C'}} = 11\,\text{m}$. Fig. 12 shows that the agreement between the proposed method and the finite element solution is excellent over the wide frequency range studied. The hydrodynamic pressure profiles are also determined using the proposed and finite element methods. Fig. 13 illustrates the profiles corresponding to frequencies $0.8\,\tilde{f}_1$ and $1.2\,\tilde{f}_1$, where $\tilde{f}_1$ denotes the coupled vibration frequency of the tank-reservoir system. These results confirm that the proposed method and advanced finite element modeling yield almost identical hydrodynamic profiles.

The seismic response of the tank-reservoir system is investigated next using the proposed and finite element techniques described above. The tank-reservoir is subjected to the horizontal component of the El Centro ground motion from Imperial Valley earthquake (1940) shown in Fig. 7. Fig. 8 illustrates the obtained nondimensionalized horizontal relative displacements $|u/u_{\text{st}}|$ at points C and C' as well as the shear forces V/F_{stat} at sections A and A', where $F_{\text{stat}} = \rho_{\text{r}} \text{g} H_{\text{r}}^2/2$ denotes the hydrostatic force as previously. Again, the time-history results confirm that the proposed procedure yields excellent results when compared to advanced finite element formulations.

4 Conclusions

This paper presented and validated an original and efficient formulation to study horizontally accelerated symmetrical and asymmetrical liquid-containing structures. The new formulation is based on a sub-structuring approach, where the flexible containing structure is modeled using finite elements, while the impulsive effects of the fluid domain are modeled analytically through interaction forces at the fluid-structure interfaces. The detailed mathematical derivations accounting for geometrical or material asymmetry of the containing structure are developed, considering both incompressible or compressible water assumptions. The proposed formulation also includes the effects of energy dissipation through reservoir bottom absorption. The technique was programmed and its application illustrated through examples highlighting the effects of geometrical and material asymmetry on the frequency- and time-domain dynamic responses of liquid-containing structures. It is seen that geometrical or material asymmetry affects the dynamic behavior of liquid-containing structures, namely in terms of frequency response functions and time history responses of various quantities of interest. The obtained impulsive hydrodynamic pressures, displacements and shear forces were illustrated and successfully validated against advanced finite element analyses. The proposed technique is formulated in such a way that it can be easily coded into a practical and computationally efficient program.

Acknowledgements

The authors would like to acknowledge the financial support of the Natural Sciences and Engineering Research Council of Canada (NSERC) and the Quebec Fund for Research on Nature and Technology (FQRNT).

Appendix A

In this appendix, we develop the equations to obtain frequency response functions $\bar{p}_0$ and $\bar{p}_j$, $j = 1 \dots m_\mathrm{s}$, for hydrodynamic pressure. For clarity and brevity, the following notation is used

$$\bar{p}_\ell(x, y, \omega) = \begin{cases} \bar{p}_0(x, y, \omega) & \text{if} \quad \ell = 0 \quad (41) \\ \bar{p}_j(x, y, \omega) & \text{if} \quad \ell = j \quad (42) \end{cases}$$

and

$$f_0^-(y) = 1\,; \qquad f_0^+(y) = 1 \quad (43)$$

$$f_j^-(y) = \psi_j^{(x)}(-b_\mathrm{r}, y)\,; \qquad f_j^+(y) = \psi_j^{(x)}(+b_\mathrm{r}, y) \quad (44)$$

Throughout this appendix, subscript ℓ can take the values 0 or j.

Using the technique of separation of variables, we show that hydrodynamic pressure can be expressed as

$$\bar{p}_\ell(x, y, \omega) = \bar{p}_{\ell\,x}(x, \omega)\, \bar{p}_{\ell\,y}(y, \omega) \quad (45)$$

Substitution into Eq. (2) yields two differential equations that can be solved for frequency response functions $\bar{p}_{\ell\,x}$ and $\bar{p}_{\ell\,y}$ as

$$\bar{p}_{\ell\,x}(x, \omega) = \gamma_1^{(\ell)}(\omega)\, \mathrm{e}^{-\kappa(\omega)\,x} + \gamma_2^{(\ell)}(\omega)\, \mathrm{e}^{\kappa(\omega)\,x} \quad (46)$$

$$\bar{p}_{\ell\,y}(y, \omega) = \gamma_3^{(\ell)}(\omega)\, \mathrm{e}^{-\mathrm{i}\,\lambda(\omega)\,y} + \gamma_4^{(\ell)}(\omega)\, \mathrm{e}^{\mathrm{i}\,\lambda(\omega)\,y} \quad (47)$$

in which λ and κ are complex frequency-dependent parameters related by

$$\kappa(\omega)^2 = \lambda(\omega)^2 - \frac{\omega^2}{C^2} \quad (48)$$

and the coefficients $\gamma_1^{(\ell)}(\omega)$, $\gamma_2^{(\ell)}(\omega)$, $\gamma_3^{(\ell)}(\omega)$ and $\gamma_4^{(\ell)}(\omega)$ are to be determined by imposing appropriate boundary conditions.

Using the transformation of Eq. (45) into Eqs. (9) and (13), we obtain the boundary conditions to be satisfied by function $\bar{p}_{\ell\,y}$ as

$$\frac{\mathrm{d}\bar{p}_{\ell\,y}}{\mathrm{d}y}(0, \omega) - \mathrm{i}\omega q\, \bar{p}_{\ell\,y}(0, \omega) = 0 \quad (49)$$

$$\bar{p}_{\ell\,y}(H_\mathrm{r}, \omega) = 0 \quad (50)$$

Substituting $\bar{p}_{\ell\,y}(y, \omega)$ by its expression in Eq. (47) into Eqs. (49) and (50) yields to a Sturm-Liouville problem with complex-valued frequency-dependent eigenvalues $\lambda_n(\omega)$ to be ob-

tained by solving the characteristic equation

$$\mathrm{e}^{2\mathrm{i}\lambda_n(\omega)H_\mathrm{r}} = -\frac{\lambda_n(\omega) - \omega q}{\lambda_n(\omega) + \omega q} \tag{51}$$

and eigenvectors

$$Y_n(y,\omega) = \frac{\Big[\lambda_n(\omega) - \omega q\Big]\mathrm{e}^{-\mathrm{i}\lambda_n(\omega)\,y} + \Big[\lambda_n(\omega) + \omega q\Big]\mathrm{e}^{\mathrm{i}\lambda_n(\omega)\,y}}{2\lambda_n(\omega)} \tag{52}$$

satisfying the orthogonality relations for $n = 1 \ldots m_\mathrm{r}$ and $s = 1 \ldots m_\mathrm{r}$

$$\int_0^{H_\mathrm{r}} Y_s(y,\omega)\, Y_n(y,\omega)\,\mathrm{d}y = \frac{\beta_n(\omega)}{2\lambda_n^2(\omega)}\,\delta_{sn} \tag{53}$$

where δ denotes the Kronecker symbol and where the parameter β_n is given by

$$\beta_n(\omega) = H_\mathrm{r}\Big[\lambda_n^2(\omega) - \omega^2 q^2\Big] + \mathrm{i}\,\omega q \tag{54}$$

Using Eqs. (45) and (46) and the eigenvectors in Eq. (52), we show that hydrodynamic pressure can be expressed as

$$\begin{aligned}\bar{p}_\ell(x,y,\omega) &= \sum_{n=1}^{\infty}\Big[\gamma_{1,n}^{(\ell)}(\omega)\,\mathrm{e}^{-\kappa_n(\omega)\,x} + \gamma_{2,n}^{(\ell)}(\omega)\,\mathrm{e}^{\kappa_n(\omega)\,x}\Big]\,Y_n(y,\omega)\\ &\approx \sum_{n=1}^{m_\mathrm{r}}\Big[\gamma_{1,n}^{(\ell)}(\omega)\,\mathrm{e}^{-\kappa_n(\omega)\,x} + \gamma_{2,n}^{(\ell)}(\omega)\,\mathrm{e}^{\kappa_n(\omega)\,x}\Big]\,Y_n(y,\omega)\end{aligned} \tag{55}$$

in which the sum is truncated to include only the first m_r reservoir modes, and where the frequency-dependent parameter κ_n is given by Eq. (48) as

$$\kappa_n(\omega) = \sqrt{\lambda_n^2(\omega) - \frac{\omega^2}{C_\mathrm{r}^2}} \tag{56}$$

The coefficients $\gamma_{1,n}(\omega)$ and $\gamma_{2,n}(\omega)$ are obtained by substituting Eq. (55) into Eqs. (46) and (47), yielding

$$\sum_{n=1}^{m_\mathrm{r}}\kappa_n(\omega)\,\Big[\gamma_{1,n}^{(\ell)}(\omega)\,\mathrm{e}^{\kappa_n(\omega)\,b_\mathrm{r}} - \gamma_{2,n}^{(\ell)}(\omega)\,\mathrm{e}^{-\kappa_n(\omega)\,b_\mathrm{r}}\Big]\,Y_n(y,\omega) = \rho_\mathrm{r} f_\ell^-(y) \tag{57}$$

$$\sum_{n=1}^{m_\mathrm{r}}\kappa_n(\omega)\,\Big[\gamma_{1,n}^{(\ell)}(\omega)\,\mathrm{e}^{-\kappa_n(\omega)\,b_\mathrm{r}} - \gamma_{2,n}^{(\ell)}(\omega)\,\mathrm{e}^{\kappa_n(\omega)\,b_\mathrm{r}}\Big]\,Y_n(y,\omega) = \rho_\mathrm{r} f_\ell^+(y) \tag{58}$$

Adding Eqs. (57) to (58) gives

$$\sum_{n=1}^{m_\mathrm{r}} 2\,\Big[\gamma_{1,n}^{(\ell)}(\omega) - \gamma_{2,n}^{(\ell)}(\omega)\Big]\kappa_n(\omega)\cosh[b_\mathrm{r}\kappa_n(\omega)]\,Y_n(y,\omega) = \rho_\mathrm{r}\Big[f_\ell^-(y) + f_\ell^+(y)\Big] \tag{59}$$

Multiplying Eq.(59) by eigenvectors $Y_n(y,\omega)$, $s = 1 \ldots m_{\rm r}$, integrating over reservoir height $H_{\rm r}$ and using trigonometric orthogonality relationships yields for each reservoir mode n

$$\gamma_{2,n}^{(\ell)}(\omega) = \gamma_{1,n}^{(\ell)}(\omega) - \frac{\rho_{\rm r} H_{\rm r} \lambda_n^2(\omega) \left[I_{\ell n}^{+}(\omega) + I_{\ell n}^{-}(\omega) \right]}{\beta_n(\omega)\, \kappa_n(\omega) \cosh[b_{\rm r}\kappa_n(\omega)]} \tag{60}$$

where the parameters $I_{\ell n}^{-}(\omega)$ and $I_{\ell n}^{+}(\omega)$ are given by

$$I_{\ell n}^{-}(\omega) = \frac{1}{H_{\rm r}} \int_0^{H_{\rm r}} f_\ell^{-}(y)\, Y_n(y,\omega)\, {\rm d}y \tag{61}$$

$$I_{\ell n}^{+}(\omega) = \frac{1}{H_{\rm r}} \int_0^{H_{\rm r}} f_\ell^{+}(y)\, Y_n(y,\omega)\, {\rm d}y \tag{62}$$

Substituting Eq. (60) into Eq. (58) yields

$$\begin{aligned} \sum_{n=1}^{m_{\rm r}} \kappa_n(\omega) \Bigg\{ & -2\, \gamma_{1,n}^{(\ell)}(\omega) \sinh[b_{\rm r}\kappa_n(\omega)] \\ & + \frac{\rho_{\rm r} H_{\rm r} \lambda_n^2(\omega) \left[I_{\ell n}^{+}(\omega) + I_{\ell n}^{-}(\omega) \right]}{\beta_n(\omega)\, \kappa_n(\omega) \cosh[b_{\rm r}\kappa_n(\omega)]}\, {\rm e}^{b_{\rm r}\kappa_n(\omega)} \Bigg\} Y_n(y,\omega) = \rho_{\rm r} f_\ell^{+}(y) \end{aligned} \tag{63}$$

Multiplying Eq.(63) by eigenvectors $Y_n(y,\omega)$, $s = 1 ... m_{\rm r}$, integrating over reservoir height $H_{\rm r}$ and using trigonometric orthogonality relationships, gives for each reservoir mode n

$$\gamma_{1,n}^{(\ell)}(\omega) = \frac{\rho_{\rm r} H_{\rm r} \lambda_n^2(\omega) \left[I_{\ell n}^{-}(\omega)\, {\rm e}^{b_{\rm r}\kappa_n(\omega)} - I_{\ell n}^{+}(\omega)\, {\rm e}^{-b_{\rm r}\kappa_n(\omega)} \right]}{2\, \beta_n(\omega)\, \kappa_n(\omega) \sinh[b_{\rm r}\kappa_n(\omega)] \cosh[b_{\rm r}\kappa_n(\omega)]} \tag{64}$$

and using Eq. (60)

$$\gamma_{2,n}^{(\ell)}(\omega) = \frac{\rho_{\rm r} H_{\rm r} \lambda_n^2(\omega) \left[I_{\ell n}^{-}(\omega)\, {\rm e}^{-b_{\rm r}\kappa_n(\omega)} - I_{\ell n}^{+}(\omega)\, {\rm e}^{b_{\rm r}\kappa_n(\omega)} \right]}{2\, \beta_n(\omega)\, \kappa_n(\omega) \sinh[b_{\rm r}\kappa_n(\omega)] \cosh[b_{\rm r}\kappa_n(\omega)]} \tag{65}$$

Substituting Eqs. (64) and (65) into Eq. (55) leads to the following expressions of hydrodynamic pressures within the vibrating reservoir

$$\bar{p}_\ell(x,y,\omega) = \rho_{\rm r} H_{\rm r} \sum_{n=1}^{m_{\rm r}} \frac{\lambda_n^2(\omega) \left[I_{\ell n}^{-}(\omega)\, X_n^{-}(x,\omega) - I_{\ell n}^{+}(\omega)\, X_n^{+}(x,\omega) \right]}{\beta_n(\omega)\, \kappa_n(\omega)\, \sinh[b_{\rm r}\kappa_n(\omega)] \cosh[b_{\rm r}\kappa_n(\omega)]}\, Y_n(y,\omega) \tag{66}$$

in which

$$X_n^{-}(x,\omega) = \cosh\left[(x - b_{\rm r})\, \kappa_n(\omega) \right] \tag{67}$$

$$X_n^{+}(x,\omega) = \cosh\left[(x + b_{\rm r})\, \kappa_n(\omega) \right] \tag{68}$$

References

ADINA (2010). “Theory and modeling guide.” Report ARD 10-7, ADINA R& D, Inc., Watertown, MA.

Balendra, T., Ang, K. K., Paramasivam, P., and Lee, S. V. (1982). “Seismic design of flexible cylindrical liquid storage tanks.” *Earthquake Engineering and Structural Dynamics*, 10(3), 477–496.

Bouaanani, N. and Lu, F. Y. (2009). “Assessment of potential-based fluid finite elements for seismic analysis of dam–reservoir systems.” *Journal of Computers and Structures*, 87(3-4), 206–224.

Chopra, A. K. (1967). “Reservoir-dam interaction during earthquakes.” *Bulletin of the Seismological Society of America*, 57(4), 675–687.

Chopra, A. K. (1968). “Earthquake behavior of reservoir-dam systems.” *ASCE Journal of the Engineering Mechanics Division*, 94(EM6), 1475–1500.

Chopra, A. K. (1970). “Earthquake response of concrete gravity dams.” *ASCE Journal of the Engineering Mechanics Division*, 96(EM4), 443–454.

Everstine, G. C. (1981). “A symmetric potential formulation for fluid-structure interaction.” *Journal of Sound and Vibration*, 79(1), 157–160.

Fenves, G. and Chopra, A. K. 1984. “Earthquake analysis and response of concrete gravity dams.” *Report No. UCB/EERC-84/10, University of California*, Berkeley, California.

Graham, E. W., Rodriguez A. M. (1952). “Characteristics of fuel motion which affect airplane dynamics.” *Journal of Applied Mechanics*, 19, 381–388.

Hall, J. F. (ed.). (1995). “Northridge earthquake of January 17, 1994: Reconnaissance report.” *Earthquake Spectra*, Supplement C to Volume 11, Vol. 1, Earthquake Engineering Research Institute, Oakland, CA.

Hanson, R. D. (1973). “Behavior of storage tanks, the Great Alaska earthquake of 1964.” *Proc., National Academy of Science*, Washington, D.C., 7, 331–339.

Haroun, M. A. (1980). “Dynamic analyses of liquid storage tanks.” *Report No. EERL 80-04, California Institute of Technology*, Pasedenas, CA.

Haroun, M. A. and Housner, G. W. (1981a). “Seismic design of liquid storage tanks.” *Journal of Technical Councils of ASCE*, 107, 191–207.

Haroun, M. A. and Housner, G. W. (1981b). “Earthquake response of deformable liquid storage tanks.” *Journal of Applied Mechanics*, 48(2), 411–418.

Haroun, M. A. and Housner, G. W. (1982). “Complications in free vibration analysis of tanks.” *Proc., ASCE Engineering Mechanics Division*, 108(5), 801–818.

Haroun, M. A. (1983). “Vibration studies and tests of liquid storage tanks.” *Earthquake Engineering and Structural Dynamics*, 11(2), 179–206.

Hoskins, L. M. and Jacobsen, L. S. (1934). “Water pressure in a tank caused by a simulated earthquake.” *Bulletin of the Seismological Society of America*, 24, 1–32.

Housner, G. W. (1957). “Dynamic pressures on accelerated fluid containers.” *Bulletin of the Seismological Society of America*, 47, 15–35.

Housner, G. W. (1963). “Nuclear reactors and earthquakes.” *Report No. TID-7024 - United States Atomic Energy Commission*, Washington, D.C.

Jacobsen, L. S. (1949). “Impulsive hydrodynamics of fluid inside a cylindrical tank and of fluid surrounding a cylindrical pier.” *Bulletin of the Seismological Society of America*, 39(3), 189–204.

Jacobson, L. S. and Ayre, R. S. (1951). “Hydrodynamic experiments with rigid cylindrical tanks subjected to transient motions.” *Bulletin of the Seismological Society of America*, 41, 313–346.

Kana, D. D. (1979). “Seismic response of flexible cylindrical liquid storage tanks.” *Nuclear Engineering and Design*, 52(1), 185–199.

Malhotra, P. K., Norwood, M. A. and Wieland, M. (2000). “Simple procedure for seismic analysis of liquid-storage tanks.” *IABSE Structural Engineering International*, 3, 197–201.

Steinbrugge, K. V. and Flores, R. (1963). “The Chilean earthquakes of May, 1960: A structural engineering viewpoint.” *Bulletin of the Seismological Society of America*, 53(2), 225–307.

Steinberg, L. J. and Cruz, A. M. (2004). “When natural and technological disasters collide: Lessons from the Turkey earthquake of August 17, 1999.” *Natural Hazards Review*, (3)5, 121–130.

Veletsos, A. S. (1974). “Seismic effects in flexible liquid storage tank.” *Proc., 5th World Conference on Earthquake Engineering*, 630–639.

Veletsos, A. S. and Yang, J. Y. (1976). “Dynamics of fixed-base liquid storage tanks.” *US-Japan Seminar for Earthquake Engineering Research*, Tokyo, Japan, 317–341.

Veletsos, A. S. and Yang, J. Y. (1977). “Earthquake response of liquid storage tanks.” *Proc., Second EMD Specialty Conference*, ASCE, Raleigh, NC, 1–24.

Werner, P. W. and Sundquist, K. J. (1949). “On hydrodynamic earthquake effects.” *Transactions of the American Geophysical Union*, 30(5), 636–657.

List of figures

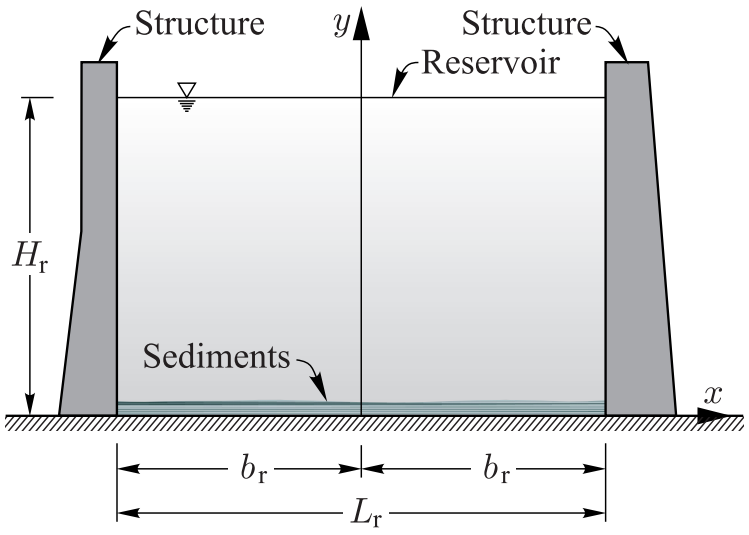

Figure 1. General geometry of the studied geometrically or materially asymmetric liquid containing structures.

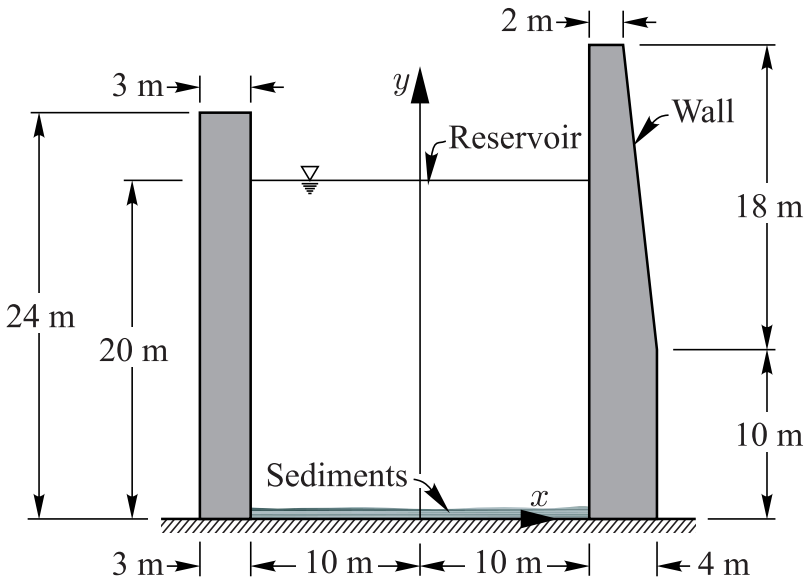

Figure 2. Geometry of the studied geometrically asymmetric wall-water system.

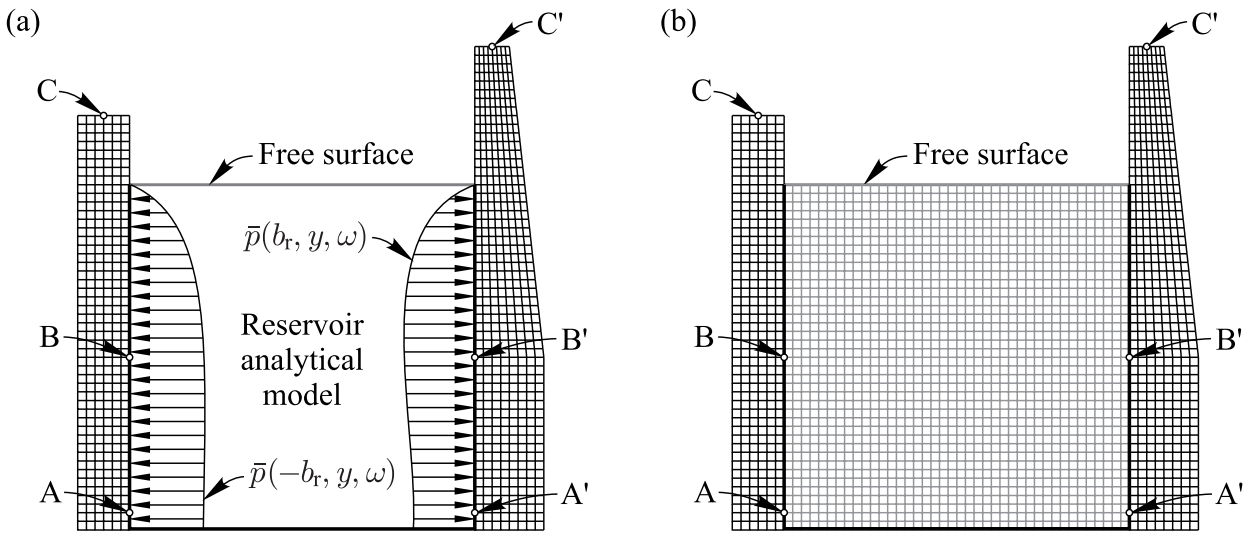

Figure 3. Geometry of the studied geometrically asymmetric wall-water system.

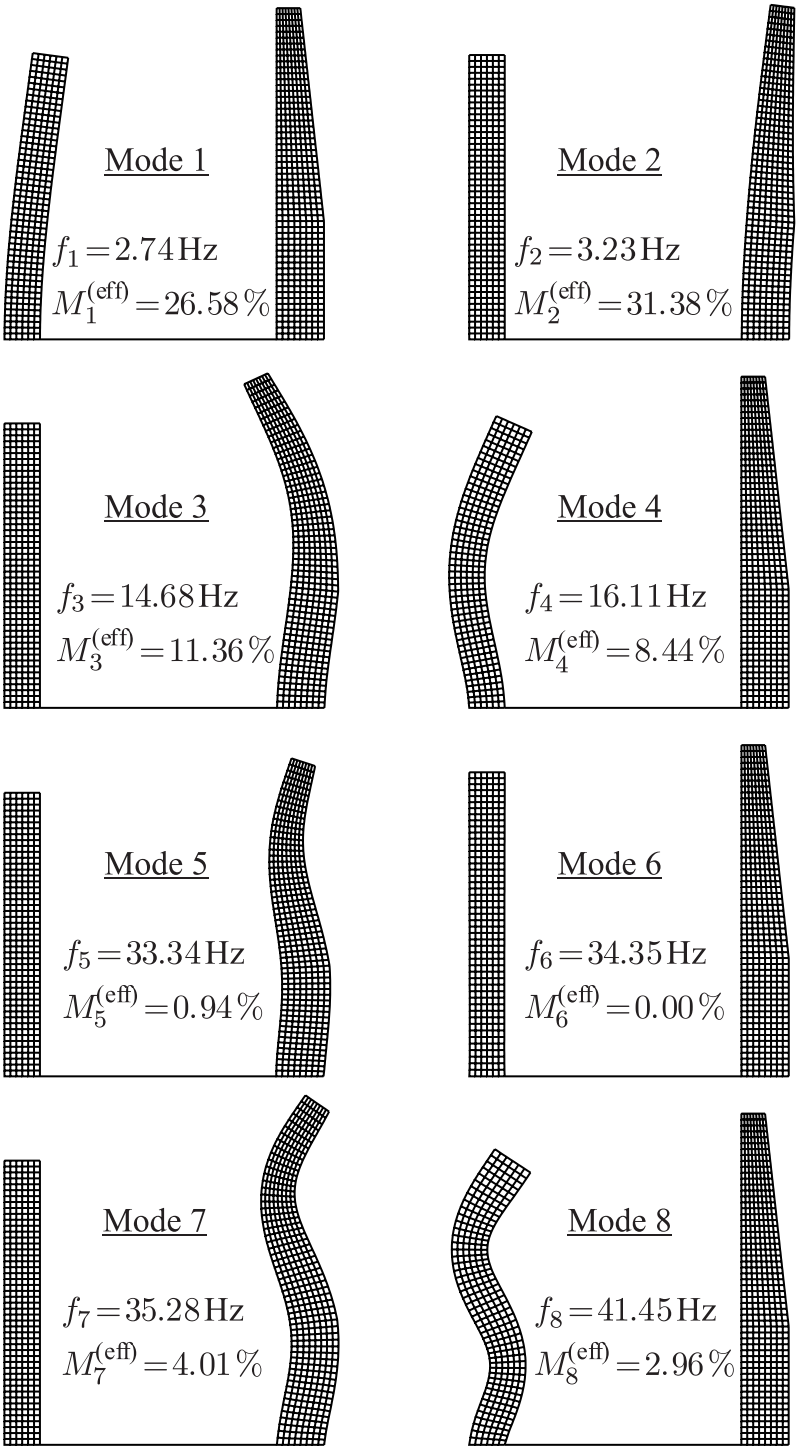

Figure 4. First eight mode shapes and corresponding frequencies and effective modal masses of the walls without water.

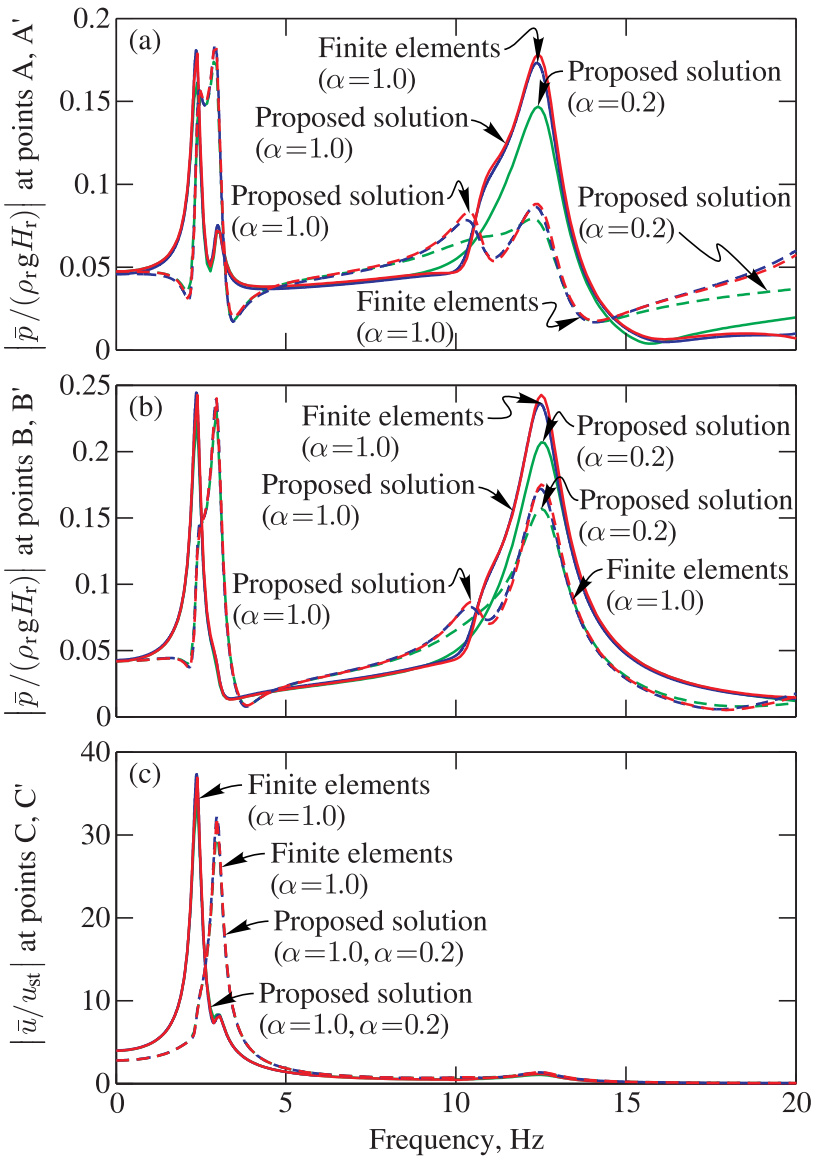

Figure 5. Nondimensionalized hydrodynamic pressures and displacements for the geometrically asymmetric wall-water system: (a) and (b) hydrodynamic pressures, (c) displacements. Continuous lines : Points A, B and C. Dotted lines : Points A', B' and C'. — Finite element solution; — Proposed solution with $\alpha = 1.0$; — Proposed solution with $\alpha = 0.2$.

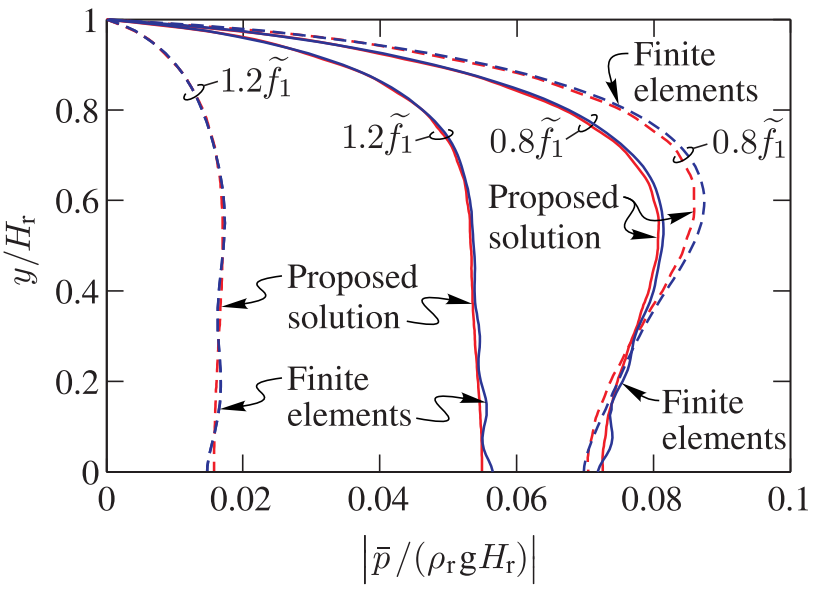

Figure 6. Nondimensionalized hydrodynamic pressure profiles on the walls of the asymmetric wall-water system. Continuous lines : Left wall. Dotted lines : Right wall. Finite element solution; Proposed solution.

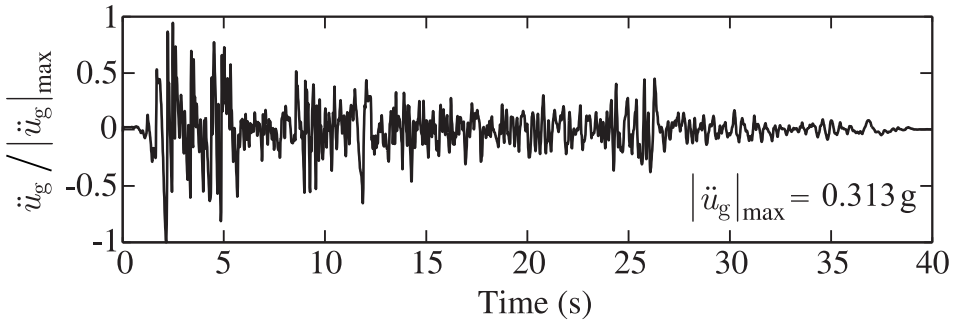

Figure 7. Horizontal acceleration component of Imperial Valley earthquake (1940) at El Centro.

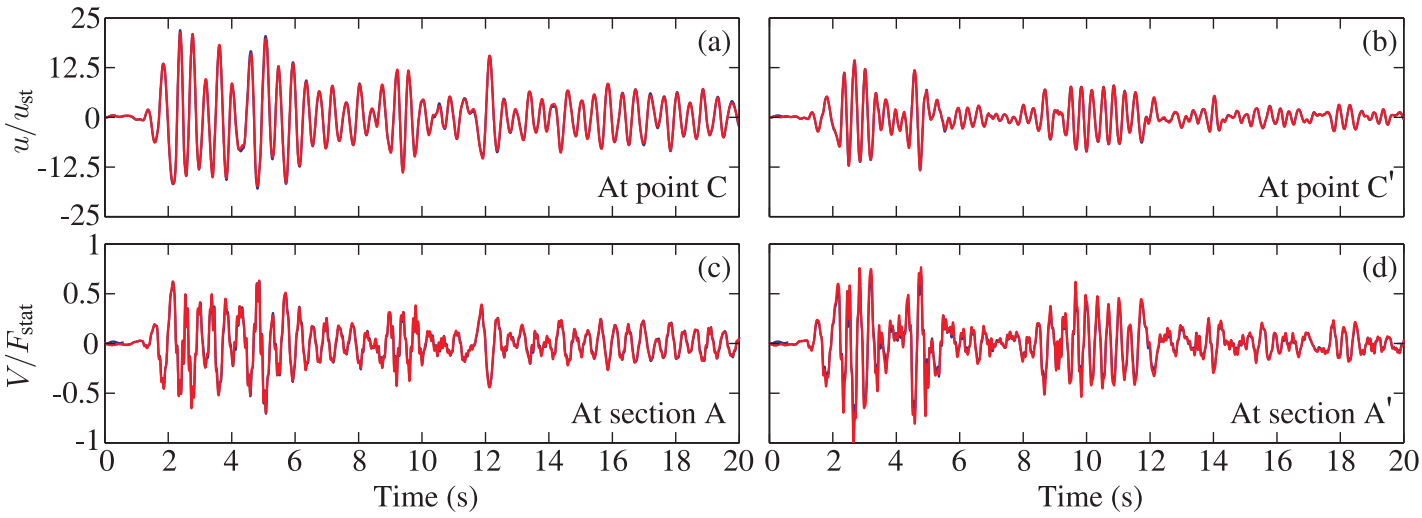

Figure 8. Time-history response of the geometrically asymmetric wall-water system: (a) Nondimensionalized displacement at point C; (b) Nondimensionalized displacement at point C'; (c) Nondimensionalized shear force at section A; (d) Nondimensionalized shear force at section A'. Finite element solution; Proposed solution.

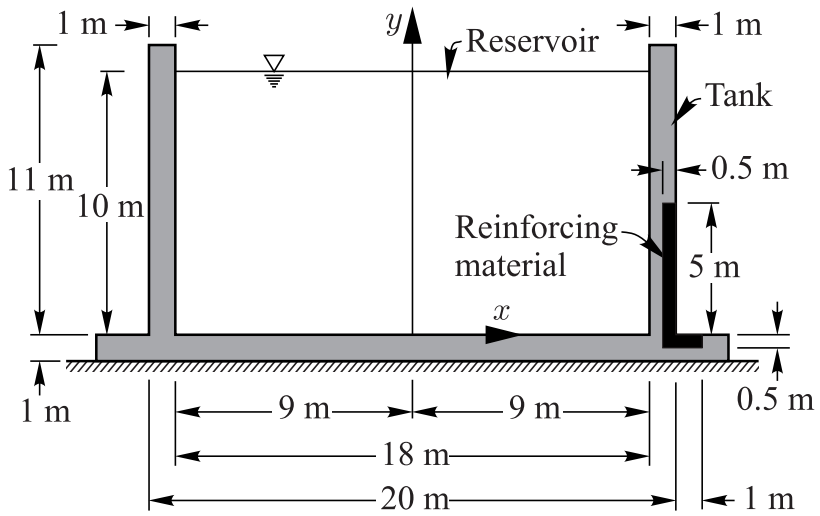

Figure 9. Geometry of the studied materially asymmetric tank-reservoir system.

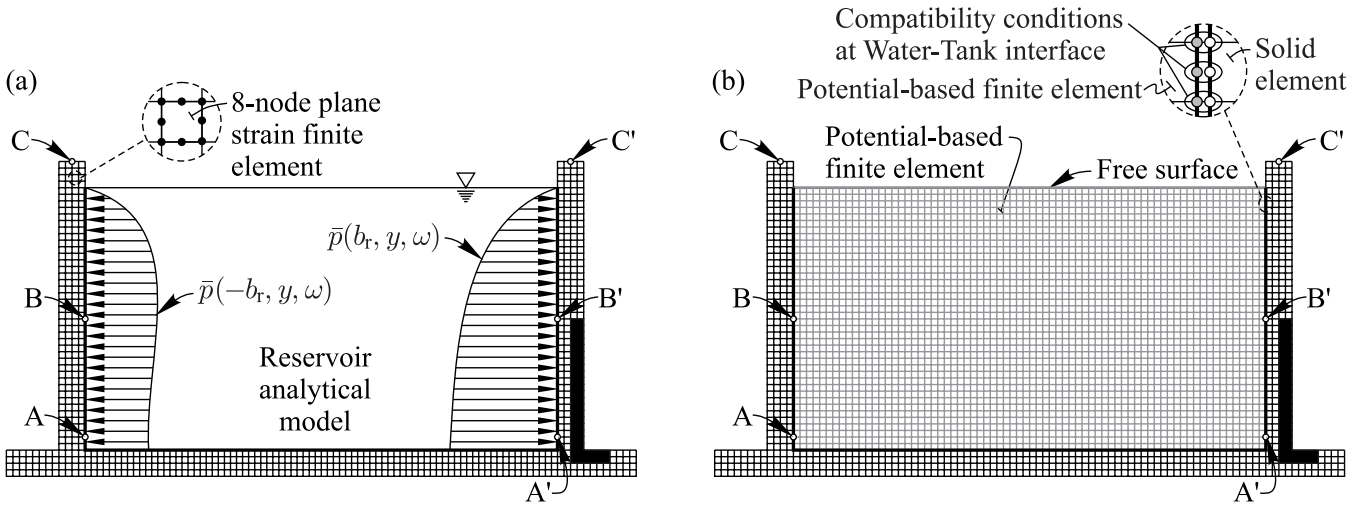

Figure 10. Finite elements models: (a) Retrofitted tank and analytical model for hydrodynamic pressure; (b) Retrofitted tank-water system.

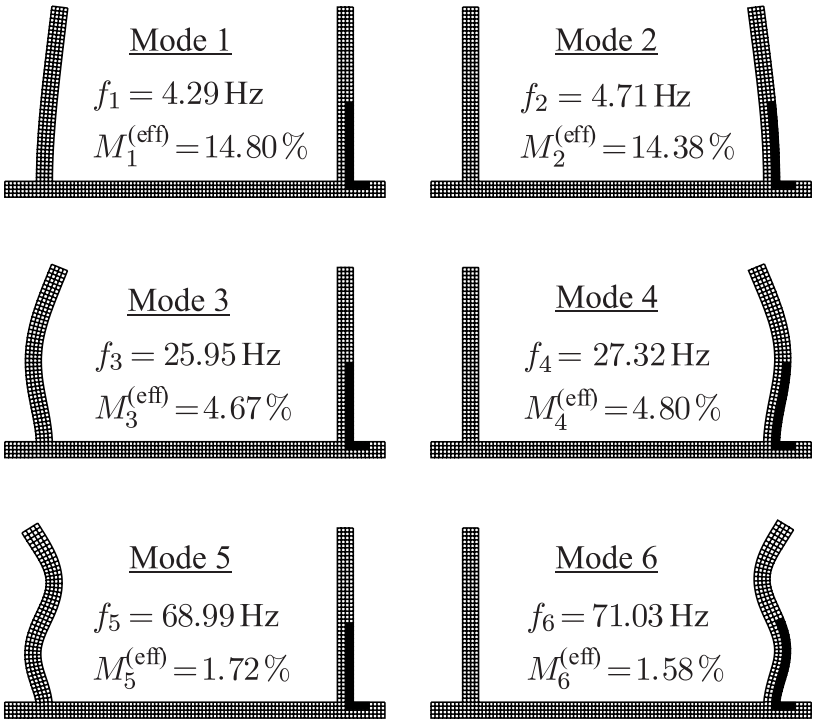

Figure 11. First six mode shapes and corresponding frequencies and effective modal masses of the asymmetrical tank.

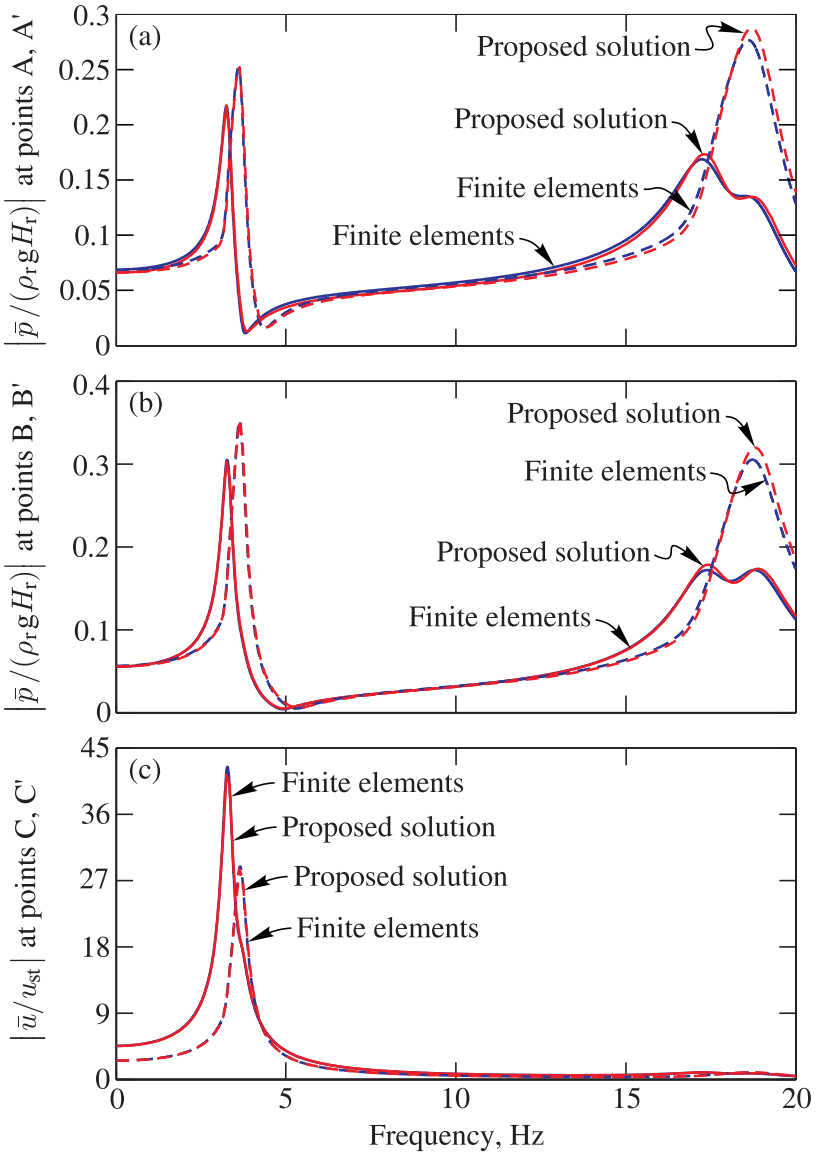

Figure 12. Nondimensionalized hydrodynamic pressures and displacements for the materially asymmetric tank-reservoir system: (a) and (b) hydrodynamic pressures, (c) displacements. Continuous lines : Points A, B and C. Dotted lines : Points A', B' and C'. — Finite element solution; — Proposed solution.

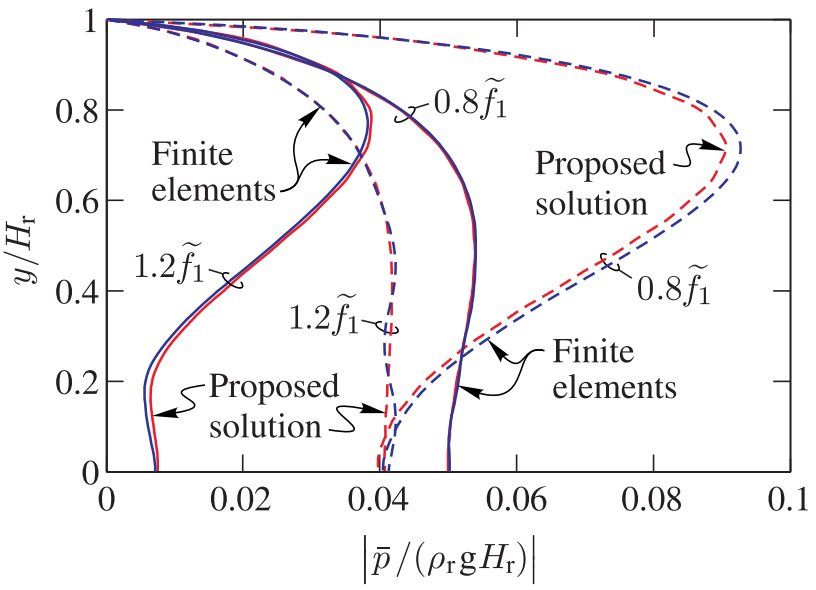

Figure 13. Nondimensionalized hydrodynamic pressure profiles on the walls of the materially asymmetric tank-teservoir system. Continuous lines : Left wall. Dotted lines : Right wall. ___ Finite element solution; ___ Proposed solution.

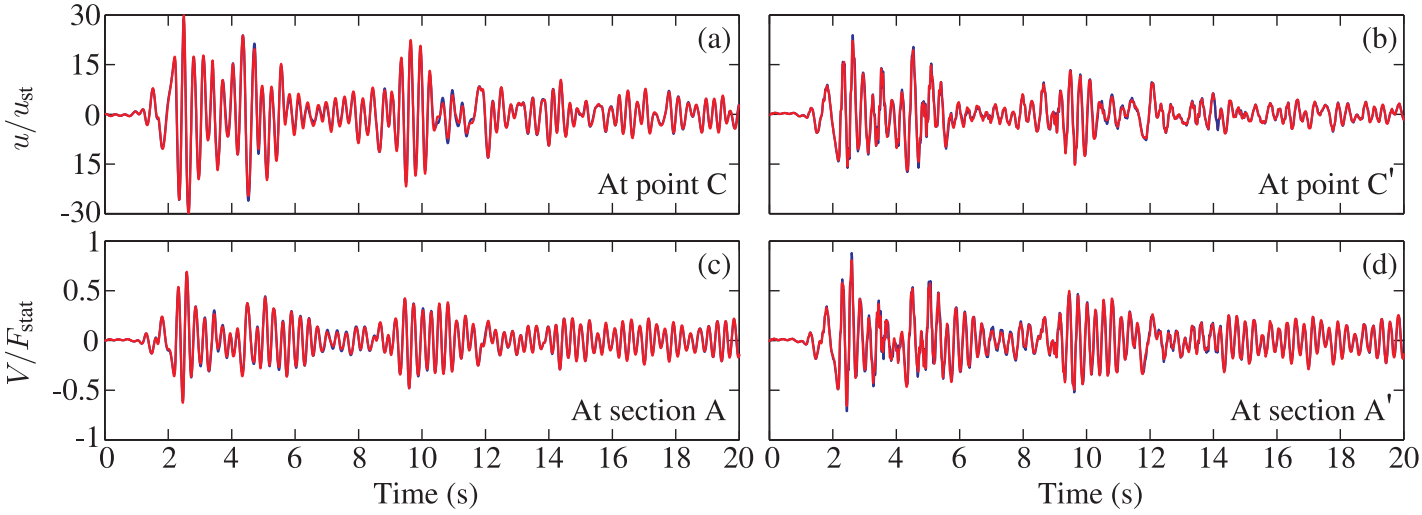

Figure 14. Time-history response of the materially asymmetric tank-reservoir system: (a) Nondimensionalized displacement at point C; (b) Nondimensionalized displacement at point C'; (c) Nondimensionalized shear force at section A; (d) Nondimensionalized shear force at section A'. ___ Finite element solution; ___ Proposed solution.